NJC

Accepted Manuscript

This is an *Accepted Manuscript*, which has been through the Royal Society of Chemistry peer review process and has been accepted for publication.

Accepted Manuscripts are published online shortly after acceptance, before technical editing, formatting and proof reading. Using this free service, authors can make their results available to the community, in citable form, before we publish the edited article. We will replace this *Accepted Manuscript* with the edited and formatted *Advance Article* as soon as it is available.

You can find more information about *Accepted Manuscripts* in the Information for Authors.

Please note that technical editing may introduce minor changes to the text and/or graphics, which may alter content. The journal's standard Terms & Conditions and the Ethical guidelines still apply. In no event shall the Royal Society of Chemistry be held responsible for any errors or omissions in this *Accepted Manuscript* or any consequences arising from the use of any information it contains.

ROYAL SOCIETY OF CHEMISTRY

www.rsc.org/njc

Fast catalytic reduction of azo dye by recoverable and reusable Fe_3O_4@PANI@Au magnetic composites

Ming Chen, Peipei Liu, Chengjiao Wang, Wenjie Ren, GuoWang Diao *

College of Chemistry and Chemistry Engineering, Yangzhou University, Yangzhou, Jiangsu, 225002, People's Republic China

Key Laboratory of Environmental Materials & Environmental Engineering of Jiangsu Province, Yangzhou, Jiangsu, 225002, P. R. China

Abstract:

In this article, a new method was applied to synthesize magnetically responsive Fe_3O_4@polyaniline (PANI) @Au nanocomposites via a three-step process. The core/shell Fe_3O_4@PANI was prepared *in situ* surface polymerization method with the assistance of sodium dodecyl sulfonate (SDS). By means of electrostatic attraction, as-prepared Au nanoparticles were adsorbed on Fe_3O_4@PANI core/shell composites to fabricate Fe_3O_4@PANI@Au composites, which were characterized by transmission electron microscopy (TEM), X-ray powder diffraction (XRD), energy-dispersive X-ray (EDX), X-ray photoelectron spectroscopy (XPS), and vibrating sample magnetometer (VSM). The catalytic activity of the Fe_3O_4@PANI@Au composites was evaluated by monitoring the reduction reaction of Congo red. Fe_3O_4@PANI@Au composite catalyst exhibited the excellent catalytic performance under low or high concentration of dye solution. The influences of electrolytes and surfactants on the catalytic reduction rate were studied. Significantly, Fe_3O_4@PANI@Au composite catalyst showed excellent catalytic performance, good stability and facile recovery by an external magnet.

Keywords: Magnetic composites, Fe_3O_4, PANI, Au nanoparticles, Dye catalytic reduction

* Corresponding Authors Tel.: +86 514 87975436, Fax: +86 514 87975244.
E-mail address: gwdiao@yzu.edu.cn (G. Daio)

Introduction

Azo dyes are synthetic organic compounds widely used in textiles, leathers, paper mill, food colorants, printing and cosmetic industries to color products. Owing to complex structure, high toxicity, long durability, poor degradability, and great solubility in water, azo dyes are considered as an important pollutant in environment. The decolorization of dye effluent has become a focus of people's attention. Dye effluent is usually treated by conventional methods such as adsorption,[1-3] coagulation,[4] electrochemical oxidation,[5] photo-catalytic degradation,[6] etc. In addition, reduction degradation is an effectively pathway including chemical reduction,[7] electroreduction [8] and bioreduction.[9,10] Because of the current efficiency of the electroreduction, the electroreduction cannot deal with huge volume and low concentration dye wastewater. Biodegradation of azo dyes is a comparatively slow procedure, which requires some redox mediators to speed up reaction rate.[9,10] Compared with electroreduction and bioreduction, chemical reduction may dispose huge volume and various concentration dye wastewater, which may become a new type of dye wastewater treatment method.

Recently, metal nanoparticles have become one of the hot topics with great popular interest originating in their unique optical,[11] electronic,[12] and catalytic properties.[13,14] In catalysis application, high catalytic activity of metal particles stems from large specific surface area and special crystalline structures. However, in many cases, the application of metallic nanostructures would encounter two major difficulties: one is the aggregation of metal nanoparticles in catalytic reaction, and the other is the separation and recovery of the catalysts in the reaction mixture. To overcome above difficulties, the immobilization of noble metal nanoparticles on a solid support has been regarded as one of the most efficient way.[15-19] These supports with high surface area and well mechanism stability, such as silica,[15,16] carbon materials,[17-19] metal oxides [20-23] and polymers,[24] are applied to immobilize nanoparticles.

The strategy would efficiently avoid the aggregation of metal nanoparticles and facilely separate catalysts from reaction system.

The application of magnetic materials as supports is a strategy to unlock above knots. Magnetic materials not only efficiently prevent the aggregation of nanoparticles, but also conveniently render the separation and recovery of nanoparticles from the reaction solution using an external magnet.[25-28] However, magnetic particles is not stability in acidic medium and may interact with catalysts or substrates, so the synthesis of composite supports with a core-shell structure has been developed to prevent magnetic particles from being corroded in acidic, base medium or reagent. Up to date, the protective shells include carbon,[29] silica,[30,31] and TiO_2.[32,33] In our previous work, Fe_3O_4@C core@shell nanocomposites were prepared and used to support Pd and Ag nanoparticles.[34,35] Safavi and Momeni synthesized palladium/hydroxyapatite/Fe_3O_4 (Pd/HAP/Fe_3O_4) nanocatalyst and evaluated its catalytic activity towards the degradation of azo dyes.[36] Pd/HAP/Fe_3O_4 was employed as a novel catalyst that offers high catalytic activity, convenient magnetic separation and good stability.

Except for inorganic materials, polymer shells on the magnetite cores not only protect the magnetite cores from damaging circumstances, but also improve the stability, water solubility and biocompatibility of the magnetic particles.[37] Among polymer shell, polyaniline (PANI) has received extensive attention due to its unique electromagnetic property. Nowadays, Fe_3O_4@PANI nanocomposite has become an important composite for applications in display devices, electromagnetic shielding, and microwave absorption material.[38-41] Fe_3O_4@PANI nanocomposites have been synthesized by several methods.[42,43] However, the study of catalytic performance of the Fe_3O_4@polymer@metal nanoaprticles three-component composites is rare and the effects of electrolytes and surfactants on the catalytic properties have little attention.

In this article, core/shell Fe_3O_4@ polyaniline (PANI) were synthesized *in situ* surface

polymerization method with the assistance of sodium dodecyl sulfonate (SDS). On the basis of electrostatic attraction, gold nanoparticles were adsorbed on Fe_3O_4@PANI composites to fabricate Fe_3O_4@PANI@Au composites. Then, the decolorization reaction of Congo red in the present of $NaBH_4$ is chosen as a model reaction to evaluate the catalytic performance of the as-prepared Fe_3O_4@PANI@Au composites. Additionally, the effects of electrolytes and surfactants on the catalytic properties were studied, which may be conducive to understand the mechanism of the heterogeneous catalysis.

Experimental Section

Materials

Hexadecyltrimethylammonium bromide (CTAB, 99+%), sodium dodecylsulfate (SDS, 99+%) and Triton X-100 were purchased from Aldrich. Other chemical reagents (analytical reagent grade) were purchased from Sinopharm Co. and used as commercial. Double distilled and sterilized water was used to prepare all solution.

Characterization

The morphology and size of specimens were characterized by transmission electron microscopy (TEM) by a Philips Tecnai-12 TEM using an accelerating voltage of 120 kV. High-resolution TEM (HRTEM) was performed on a FEI Tecnai G2 F30 S-TWIN (USA) operating at 200 kV. The X-ray powder diffraction (XRD) was performed on a D8 Advance X-ray diffractometer (Brucker, Germany) operated at a voltage of 40 kV and a current of 40 mA with Cu Kα radiation. The Energy-dispersive X-ray (EDX) analysis was performed on a KEVEX X-ray energy detector. The X-ray photoelectron spectroscopy (XPS) experiments were carried out on a Thermo Escalab 250 system using Al Kα radiation ($h\nu$= 1486.6 eV). The test chamber pressure was maintained below 2×10^{-9} Torr during spectral acquisition. The

magnetic measurement were carried out on a vibrating sample magnetometer (VSM, EV7, ADE, USA) with an applied field between -8000 and 8000 Oe at room temperature. FTIR spectra for the different samples were recorded on a Bruker TENSOR 27 FTIR spectrometer operated at a resolution of 4 cm^{-1}. The Au loading amount was determined by inductively couple plasma mass spectrometry (ICP-MS, Elan DRC-e, PerkinElmer Com.). The UV-vis spectra were taken by a Shimazu UV-2501 double-beam spectra photometer.

Synthesis of Fe_3O_4@PANI@Au Nanocomposites

As illustrated in Fig. 1, the overall procedure for the preparation of the Fe_3O_4@PANI@Au catalyst includes three steps. Firstly, Fe_3O_4 microspheres were prepared via a solvothermal method referred to our previous report.[44] Secondly, we used a new strategy to prepare Fe_3O_4-PANI core/shell structure. A thin PANI layer was coated on the surface of the pre-synthesized Fe_3O_4 microspheres to form Fe_3O_4@PANI composites through *in situ* polymerization in the presence of sodium dodecyl sulfonate (SDS, anionic surfactant). SDS would adsorb on the surface of Fe_3O_4 microspheres, resulting in negatively charged surface of Fe_3O_4 microspheres. Then, the positive charged aniline monomers in acid condition absorbed on the surface of Fe_3O_4 microspheres through Coulombic force between —OSO_3^- of SDS and aniline cation. Under initiator, *in situ* oxidative polymerization of aniline monomers will react on the surface of Fe_3O_4 microspheres. In a typical procedure, as-prepared dried Fe_3O_4 (0.1 g) and SDS (5 mg) was suspended in 100 mL distilled water under ultrasonic irradiation and mechanical stirring. After 2 h, aniline (50 μL) in the presence of concentrated HCl (0.1 mol/L, 10 mL) was added into the mixture at 0 ^oC (ice-water bath). The solution was mechanical stirred for 2 h in ice-water bath. Ammonium peroxodisulfate (APS) aqueous solution (0.5 g of APS in 5 mL of H_2O) was added into the above mixture to initiate polymerization reaction under mechanical agitation. The reaction was carried out 12 h at room temperature. Finally,

the Fe_3O_4@PANI composites were separated by an external magnetic field, rinsed successively with H_2O and ethanol three times and dried in vacuum for 12 h at 60 ^oC.

Thirdly, by virtue of multiple electrostatic interactions,[45] as-prepared Au nanoparticles were immobilized on Fe_3O_4@PANI core/shell composites used as a support or carrier to generate Fe_3O_4@PANI@Au composites. In detail, the Fe_3O_4@PANI composites (0.1 g/mL, 2 mL) were sonicated at room temperature for 0.5 h. Then, a colloid solution of Au nanoparticles (an average diameter 5 nm) was prepared according to the literature reported by Grabar.[46] Subsequently, the solution of Fe_3O_4@PANI composites was added to the freshly prepared Au solution (100 mL) under sonication at room temperature for 20 min. Gold nanoparticles were electrostatically anchored onto the surface of the Fe_3O_4@PANI composites; thereby, the resultant Fe_3O_4@PANI@Au composites were separated from the solution using an external magnetic field. The products were washed successively with H_2O and ethanol three times and dried under vacuum at 60 ^oC.

Catalytic property of Fe_3O_4@PANI@Au Nanocomposites

Fe_3O_4@PANI@Au catalysts (10 mg) were added into Congo red aqueous solution (20 mL, 6.0×10^{-5} mol/L). Then, fresh $NaBH_4$ solution (1.5 mL, 0.1 mol/L) was mixed with above solution. Under continuous stirring, the reaction was carried out at 25 ^oC. The process of the decolorization reaction was recorded by a UV-vis absorption spectrophotometer. When the reaction was completed, the catalysts were facilely separated from solution via an external magnet.

Results and discussion

Characterization of Fe_3O_4@PANI@Au catalyst

The overall procedure for the preparation of the Fe_3O_4@PANI@Au catalyst contains three

steps. The Fe_3O_4 core was prepared via a solvothermal method. Then, PANI shell was coated on the surface of Fe_3O_4 to form Fe_3O_4@PANI composites through in situ polymerization with the assistance of SDS. Lastly, as-prepared Au nanoparticles were adsorbed on PANI shell to form Fe_3O_4@PANI@Au composites by virtue of electrostatic interactions. The morphologies of specimens at different step were firstly characterized by TEM. TEM image in Fig. 2a shows the Fe_3O_4 microspheres with average diameters of 300 nm. In Fig. 2b, it is obvious that PANI coated Fe_3O_4 microspheres are perfectly spherical in shape with smooth surfaces and well-defined core@shell structures. The core@shell Fe_3O_4@PANI composites are uniform with a diameter of ~ 350 nm, and the shell layer of PANI is ~ 25 nm in thickness. When the Fe_3O_4@PANI nanocomposites are introduced into the Au colloid solution, Fe_3O_4@PANI@Au composite microspheres are formed by virtue of multiple electrostatic interactions. The corresponding TEM images are shown in Fig. 2c. For better understanding of the size and dispersion of Au nanoparticles on the shell of PANI, high-resolution transmission electron microscopy (HRTEM) was recorded. In Fig, 2d, it is clear that the thickness of PANI shell is about 25 nm and Au nanoparticles are homogeneously embedded in the shell layer of PANI without forming large aggregation. No individual nanoparticles are observed in the residual solution. In Fig. 2e, the average diameter of Au nanoparticles is about 5 nm. The lattice resolved HRTEM image of Au nanoparticle is shown in Fig. 2f. Inter planar spacing of 2.34 nm corresponds well with Au (111) plane. Furthermore, Fe_3O_4@PANI@Au composites have no disintegration even after an ultrasound for 0.5 h, which indicates these hybrid composites have the stable structures.

Fig. 3 showed the XRD patterns of the Fe_3O_4 microspheres, Fe_3O_4@PANI composites and Fe_3O_4@PANI@Au composites. In Fig. 3a, all of peaks are attributed to the orthorhombic phase of Fe_3O_4. After coating PANI shell, the peaks have no obvious changes compared with Fe_3O_4 microspheres (Fig. 3b). In Fig. 3c, the typical XRD pattern of Fe_3O_4@PANI@Au

nanocomposites has no the characteristic peaks of Au nanoparticles. Because the amount of Au nanoparticles loaded onto thin PANI layer is smaller than that of Fe_3O_4, the intensity of diffraction peaks of Fe_3O_4 in Fe_3O_4@PANI@Au is much stronger than that of Au nanoparticles, resulting into the absence of Au diffraction peaks in Fe_3O_4@PANI@Au nanocomposites.

To confirm Au nanoparticles anchoring on the surface of Fe_3O_4@PANI, EDX and XPS were used to characterize Fe_3O_4@PANI@Au nanocomposites. The EDX result in Fig. 4A shows that the main elemental compositions of the nanocomposites are C, N, O, Fe and Au. The result indicates that Au nanoparticles are well-absorbed onto the Fe_3O_4@PANI composites to generate the Fe_3O_4@PANI@Au nanocomposites. The atom ratios Au:Fe of in Fe_3O_4@PANI@Au nanocomposites is determined to be 1:42 by EDX. The corresponding weight fraction of Au nanoparticles in nanocomposites is 4.0 %, which is close to the value (3.8%) determined by ICP-MS. To further demonstrate the composition of the shell, XPS was employed to analyze Fe_3O_4@PANI@Au nanocomposites. It is clear that the four elements of C, O, N, and Au exist in the surface. Obviously, the signals of Au are much stronger than other elements (C, O and N) in Fig. 4B. This phenomenon results from the dense cover of Au nanoparticles on the shell PANI layer. XPS result is consistent with TEM observation. However, the binding energy at 712.3 eV and 726.2 eV for Fe $2p^{3/2}$ and Fe $2p^{1/2}$ cannot be detected,[35] which indicates that Fe_3O_4 cores are wrapped in shells of PANI@Au. In addition, the binding energy at 695.6 eV for F 1s may come from the teflon reactor. Therefore, on the basis of the results of XRD, EDX and XPS, Fe_3O_4@PANI@Au nanocomposites have been successfully prepared.

Fig. 5A shows the FTIR spectra of (a) Fe_3O_4 microspheres, (b) core@shell Fe_3O_4@PANI composites, and (c) Fe_3O_4@PANI@Au composites. In curve a, the strong absorption peak at 576 cm^{-1} corresponds to the Fe—O vibrations. The characteristic peaks at approximately 1596,

1496, 1316, 1149, and 831 cm^{-1} in curve b are similar to that of the pure PANI sample, confirming that the PANI shell is successfully coated on the surface of Fe_3O_4 microspheres. In curve c, the typical FTIR spectrum of Fe_3O_4@PANI@Au is similar to the spectrum of Fe_3O_4@PANI composites.

The magnetic properties of Fe_3O_4 microspheres, core@shell Fe_3O_4@PANI composites, and Fe_3O_4@PANI@Au catalysts were investigated by VSM at room temperature and shown in Fig. 5B. All of samples exhibit ferromagnetic behavior at room temperature. The saturated magnetization (Ms) values of Fe_3O_4, Fe_3O_4@PANI, and Fe_3O_4@PANI@Au are 77.1, 58.6 and 39.2 emu/g, respectively. The hysteresis loop of the as-prepared Fe_3O_4 microspheres is similar to our previous report.[44] After PANI shell packing Fe_3O_4 (curve b), the saturated magnetization of core@shell Fe_3O_4@PANI composite decreases because of the shield of PANI layer. It is noted that the saturated magnetization of Fe_3O_4@PANI@Au composites decreases considerably with the immobilization of Au nanoparticles on the support of Fe_3O_4@PANI (curve c). However, it is fortunate that the magnetism of Fe_3O_4@PANI@Au composites is still strong enough to be separated easily from solution with the assistance of an external magnetic field.

Catalytic Properties of Fe_3O_4@PANI@Au catalyst

To evaluate the catalytic property of the as-prepared Fe_3O_4@PANI@Au catalyst, the decolorization reaction of Congo red in the present of $NaBH_4$ is chosen as a model reaction. In the control experiment, the color of Congo red solution with large excess of $NaBH_4$ remained unchanged for 2 h, which indicated that the reduction reaction rate was extremely slow without the assistance of catalyst. However, when Fe_3O_4@PANI@Au catalyst was added in above reaction system, the color of Congo red disappeared within 3 minutes, demonstrating the catalytic property of Fe_3O_4@PANI@Au for the fast reduction of Congo red.

Effect of the Concentration of $NaBH_4$ on Catalytic Properties

The concentration of $NaBH_4$ has a profound impact on the catalytic reduction rate of Congo red. Fig. 6 shows the UV-vis spectra of Congo red with different concentration of $NaBH_4$ in the presence of Fe_3O_4@PANI@Au catalyst at 25 ^oC. The catalytic reduction rate of Congo red increased with the increase concentration of $NaBH_4$. When the concentration of $NaBH_4$ was 5×10^{-3} mol/L, the whole decolorization process required 53 min. However, the solution changed to colorless within 6 min in 9×10^{-3} mol/L $NaBH_4$ solution. The pseudo first-order kinetic equation is applied to fit the data obtained from Fig. 6C. The linear relation between $\ln(c_t/c_0)$ and reaction time is displayed in Fig. 6D, from which the reaction rate constant is calculated to be 0.80 min^{-1} at 25 ^oC. To monitor the decline of absorbance of Congo red with time, follow-up studies adopted a moderate reaction system. The concentration of $NaBH_4$ was 7×10^{-3} mol/L (1.5 mL, 0.1 mol/L $NaBH_4$ added into reaction system). Compared with other supported Au nanoparties in the reported literatures, the Fe3O4@PANI@Au composite displayed the good catalyst performance. Wu's group reported that Au@polypyrrole/Fe_3O_4 hollow capsules catalyzed reduction of methylene blue with the rate constant (k= 0.266 min^{-1}).[47] Au-loaded Fe_3O_4@C composite microspheres were used to catalyze reduction of methylene blue. The largest rate constant was 0.331 min^{-1}.[48]

When the initial concentration of Congo red increased 10 times, the catalytic performance of Fe_3O_4@PANI@Au composite was studied. Fig. 7A shows the UV-vis spectra of high concentration of Congo red with the reduction of $NaBH_4$ in the presence of Fe_3O_4@PANI@Au catalyst at 25 ^oC. Before UV-vis spectra test, the solutions were diluted 10 times. Under the experiment condition, the solution changed to colorless within 20 min. From Fig. 7B, the reaction rate constant is calculated to be 0.18 min^{-1} at 25 ^oC, which indicates that Fe_3O_4@PANI@Au catalyst still exhibits the excellent catalytic performance even under the

high concentration of dye.

Influence of Electrolytes on Catalytic Properties of Fe_3O_4@PANI@Au

The catalytic properties of catalysts are frequently influenced by external circumstances, such as electrolytes and surfactants, so we researched the impacts of electrolytes and surfactants on Fe_3O_4@PANI@Au catalysts. Fig. 8A shows the change of absorbance with the reaction time in the addition of different salts. It is clear that the catalytic properties of Fe_3O_4@PANI@Au depended largely on the natural instincts of these electrolytes. In Fig. 8A, sodium nitrate and sodium sulfate increased the catalyzed reduction of the dyes. However, the catalytic reduction rate was decreased in Na_3PO_4 solution. Generally speaking, electrolytes have two aspects of influence on the catalytic properties of catalysts. In a good way of course, electrolytes might facilitate the charges migration. The rapidity of charges migration will be conducive to the increase of the catalytic rate. In the adverse side, electrolytes might adsorb onto the surface of catalysts and block active sites, resulting in catalyst passivation due to preferential adsorption of the electrolytes.[49] In this case, $NaNO_3$ and Na_2SO_4 mainly display the positive effect. The promotion of the charges migration of two salts predominates during the catalytic reaction. Oppositely, a slow catalytic reaction rate was presented due to the adsorption of PO_4^{3-} on Au nanoparticles.[50] Niaura et al., confirmed the monodentate surface coordination of the PO_4^{3-} on gold electrode by surface-enhanced Raman spectroscopy.[50] Furthermore, in Fig. 8B, the catalyzed reduction rates of the dyes decrease with an increase in the electrolyte concentration of $NaNO_3$, but the catalyzed reduction rates were still larger than that without addition electrolytes. With the increase of $NaNO_3$ concentration, adsorption of salt onto the surface of Au nanoparticles turned into the main influence factor gradually and rendered the decrease of the catalytic reduction rate of dyes.

Influence of Surfactants on Catalytic Properties of Fe_3O_4@PANI@Au

Since large amounts of surfactants exist in dye wastewater, it is necessary to study the effects of surfactants on the catalysis reduction of dyes. In this case, three kinds of representative surfactants were applied to study the effects on the catalyzed reduction. Compared to the reduction rate without surfactants in the solution, the addition of surfactants brought about obvious decrease of the reduction rates in Fig. 9. The order of the reduction rate of the dyes is no surfactant > TX-100 > SDS > CTAB. In general, surfactants tend to adsorb on the surface of metal nanoparticles and hinder the accessibility to the active sites on metal nanoparticles for reaction molecules.[49] The stronger adsorption of surfactants leads to the loss of catalytic activity of catalysts and the inaccessibility to the active sites on Au nanoparticles for reaction molecules (BH_4^-). In most cases, the surface of metal nanoparticles is negative charge, so cationic surfactants more easily adsorb on metal nanoparticles and occupy more catalytic active centers, resulting in the considerable decrease of reaction rate. Thus, the reduction rate of Congo red in the presence of CTAB is the smallest in three surfactants. Furthermore, if surfactants and reaction molecules have the same charge, electrostatic repulsion also affects the accessibility to Au nanopaticles for reacting molecules. In this case, because BH_4^-, Congo red and SDS take the same charge, electrostatic repulsion would prevent BH_4^- and Congo red from accessing to Au nanoparticles. Therefore, in Fig. 9, the reduction rate of Congo red in the presence of SDS is smaller than that in TX-100.

Stability and recycling of the catalyst

The renewable catalytic activity, another important parameter for the recyclable catalyst, was also researched in this paper. The advantage of magnetic catalysts is the convenient separation and recovery from the reaction solution using an external magnet (as shown in Fig. 10A). When the reaction was completed, the catalysts were facilely separated out by using a

magnet. Then, the catalysts were rinsed with H_2O and ethanol three times and dried for the next cycle of catalysis. As shown in Fig. 10B, the decolorization (%) of reduction reaction almost maintained constant after five cycles, which confirmed that Fe_3O_4@PANI@Au composite catalyst displayed excellent catalytic activity and good stability. In order to confirm the stability of the catalyst, the catalyst after five cycles was analyzed by TEM and ICP-MS. In inset of Fig. 10A, no discernible change of Au nanoparticles was observed, indicating that Au nanoparticles supported on Fe_3O_4@PANI sphere were sufficiently stable and no aggregation took place after five cycles of the catalysis reaction. After five cycles, the result of ICP-MS showed determinable Au loss, but the loss amount was trace and about 5 %, which implied the high affinity between Au nanoparticles and Fe_3O_4@PANI supports, and the good performance of the magnetic separation in the present catalytic system.

Conclusions

In this article, Fe_3O_4@PANI@Au composites exhibiting both excellent magnetic and catalytic properties were successfully fabricated via a three-step procedure. The catalytic properties of Fe_3O_4@PANI@Au composite were investigated by the reduction of Congo red with $NaBH_4$. Fe_3O_4@PANI@Au composite catalyst showed the excellent catalytic performance for various concentration dye wastewater. The catalytic properties of Fe_3O_4@PANI@Au depended largely on the natural instincts of electrolytes. Surfactants will render the catalysts passivation, resulting in the decrease the reaction rate. Immobilization of Au nanoaprticles onto Fe_3O_4@PANI core/shell composites effectively prevented nanoparticles from aggregating, thus improving the stability of catalysts and achieving the facile recovery of the catalysts from the reaction solution. Most importantly, dye catalytic reduction by magnetic composites may be a potential and effective pathway to decolor huge volume and various concentration dye wastewater.

Acknowledgements

This work was financially supported by the National Natural Science Foundation of China (Grant No. 21273195), a Project Funded by the Priority Academic Program Development of Jiangsu Higher Education Institutions, and the Natural Science Foundation of Education Committee of Jiangsu Province (12KJB150023). The work was also sponsored by Qing Lan Project of Higher Learning Institutions in Jiangsu Province and Jiangsu Key Laboratory of Environmental Material and Environmental Engineering (K13062). The authors also acknowledge the Testing Center of Yangzhou University for TEM, HRTEM, XRD and EDX experiments.

References

1. M. Rafatullah, O. Sulaiman, R. Hashim, and A. Ahmad, *J. Hazard. Mater.*, 2010, **177**, 70.
2. M. Chen, Y. Chen, and G. Diao, *J. Chem. Eng. Data*, 2010, **55**, 5109.
3. M. Chen, T. Shang, W. Fang, and G. Diao, *J. Hazard. Mater.*, 2011, **185**, 914.
4. J.-W. Lee, S.-P. Choi, R. Thiruvenkatachari, W.-G. Shim, and H. Moon, *Dyes Pigments*, 2006, **69**, 196.
5. M. Chen, W. Ding, J. Wang, and G. Diao, *Ind. Eng. Chem. Res.*, 2013, **52**, 2403.
6. J. P. Ghosh, R. Sui, C. H. Langford, G. Achari, and C. P. Berlinguette, *Water Res.*, 2009, **43**, 4499.
7. W. Zhang, F. Tan, W. Wang, X. Qiu, X. Qiao, and J. Chen, *J. Hazard. Mater.*, 2012, **217–218**, 36.
8. Y. Tian, L. Huang, X. Zhou, and C. Wu, *J. Hazard. Mater.*, 2012, **225–226**, 15.
9. F. P. van der Zee, I. A. E. Bisschops, G. Lettinga, and J. A. Field, *Environ. Sci. Technol.*, 2003, **37**, 402.
10. G. Mezohegyi, A. Kolodkin, U. I. Castro, C. Bengoa, F. Stuber, J. Font, A. Fabregat, and A. Fortuny, *Ind. Eng. Chem. Res.*, 2007, **46**, 6788.
11. K. L. Kelly, E. Coronado, L. L. Zhao, and G. C. Schatz, *J. Phys. Chem. B*, 2003, **107**, 668.
12. A. N. Shipway, E. Katz, and I. Willner, *Chemphyschem*, 2000, **1**, 18.
13. N. Lopez, T. V. W. Janssens, B. S. Clausen, Y. Xu, M. Mavrikakis, T. Bligaard, and J. K.

Nørskov, *J. Catal.*, 2004, **223**, 232.

14. J. D. Aiken III and R. G. Finke, *J. Mol. Catal. Chem.*, 1999, **145**, 1.
15. A. K. Sinha, S. Seelan, S. Tsubota, and M. Haruta, *Angew. Chem. Int. Ed.*, 2004, **43**, 1546.
16. J. Lee, J. C. Park, and H. Song, *Adv. Mater.*, 2008, **20**, 1523.
17. S. H. Joo, S. J. Choi, I. Oh, J. Kwak, Z. Liu, O. Terasaki, and R. Ryoo, *Nature*, 2001, **412**, 169.
18. V. Georgakilas, D. Gournis, V. Tzitzios, L. Pasquato, D. M. Guldi, and M. Prato, *J. Mater. Chem.*, 2007, **17**, 2679.
19. C. Xu, X. Wang, and J. Zhu, *J. Phys. Chem. C*, 2008, **112**, 19841.
20. S. Ivanova, C. Petit, and V. Pitchon, *Appl. Catal. Gen.*, 2004, **267**, 191.
21. J. Sun, Z. Dong, X. Sun, P. Li, F. Zhang, W. Hu, H. Yang, H. Wang, and R. Li, *J. Mol. Catal. Chem.*, 2013, **367**, 46.
22. G. J. Hutchings, M. S. Hall, A. F. Carley, P. Landon, B. E. Solsona, C. J. Kiely, A. Herzing, M. Makkee, J. A. Moulijn, A. Overweg, J. C. Fierro-Gonzalez, J. Guzman, and B. C. Gates, *J. Catal.*, 2006, **242**, 71.
23. S. Li, W. Zhang, M.-H. So, C.-M. Che, R. Wang, and R. Chen, *J. Mol. Catal. Chem.*, 2012, **359**, 81.
24. H. Dong, E. Fey, A. Gandelman, and W. E. Jones, *Chem. Mater.*, 2006, **18**, 2008.
25. A. Hu, G. T. Yee, and W. Lin, *J. Am. Chem. Soc.*, 2005, **127**, 12486.
26. A.-H. Lu, E. L. Salabas, and F. Schüth, *Angew. Chem. Int. Ed.*, 2007, **46**, 1222.
27. P. D. Stevens, G. Li, J. Fan, M. Yen, and Y. Gao, *Chem. Commun.*, 2005, 4435.
28. X. Deng, K. Lin, X. Chen, Q. Guo, and P. Yao, *Chem. Eng. J.*, 2013, **225**, 656.
29. Z. Chen, Z. Xue, L. Chen, Z. Geng, R. Yang, L. Chen, and Z. Wang, *New J. Chem.*, 2013, **37**, 3731.
30. G. Wang, L. Jin, Y. Dong, L. Niu, Y. Liu, F. Ren, and X. Su, *New J. Chem.*, 2014, **38**, 700.
31. L. Sun, Y. Li, M. Sun, H. Wang, S. Xu, C. Zhang, and Q. Yang, *New J. Chem.*, 2011, **35**, 2697.
32. R. Chalasani and S. Vasudevan, *ACS Nano*, 2013, **7**, 4093.
33. T. Xin, M. Ma, H. Zhang, J. Gu, S. Wang, M. Liu, and Q. Zhang, *Appl. Surf. Sci.*, 2014, **288**, 51.
34. M. Zhu and G. Diao, *J. Phys. Chem. C*, 2011, **115**, 24743.
35. M. Zhu, C. Wang, D. Meng, and G. Diao, *J. Mater. Chem. A*, 2013, **1**, 2118.

36. A. Safavi and S. Momeni, *J. Hazard. Mater.*, 2012, **201–202**, 125.
37. K. Shang, B. Sun, J. Sun, J. Li, and S. Ai, *New J. Chem.*, 2013, **37**, 2509.
38. J. Deng, X. Ding, W. Zhang, Y. Peng, J. Wang, X. Long, P. Li, and A. S. C. Chan, *Polymer*, 2002, **43**, 2179.
39. J. Deng, C. He, Y. Peng, J. Wang, X. Long, P. Li, and A. S. C. Chan, *Synth. Met.*, 2003, **139**, 295.
40. S. S. Umare, B. H. Shambharkar, and R. S. Ningthoujam, *Synth. Met.*, 2010, **160**, 1815.
41. C. Yang, J. Du, Q. Peng, R. Qiao, W. Chen, C. Xu, Z. Shuai, and M. Gao, *J. Phys. Chem. B*, 2009, **113**, 5052.
42. S. Xuan, Y.-X. J. Wang, K. C.-F. Leung, and K. Shu, *J. Phys. Chem. C*, 2008, **112**, 18804.
43. S. Xuan, Y.-X. J. Wang, J. C. Yu, and K. C.-F. Leung, *Langmuir*, 2009, **25**, 11835–11843.
44. M. Zhu and G. Diao, *J. Phys. Chem. C*, 2011, **115**, 18923.
45. H. Zhang, X. Zhong, J.-J. Xu, and H.-Y. Chen, *Langmuir*, 2008, **24**, 13748.
46. K. C. Grabar, K. J. Allison, B. E. Baker, R. M. Bright, K. R. Brown, R. G. Freeman, A. P. Fox, C. D. Keating, M. D. Musick, and M. J. Natan, *Langmuir*, 1996, **12**, 2353.
47. T. Yao, T. Cui, H. Wang, L. Xu, F. Cui, and J. Wu, *Nanoscale*, 2014, **6**, 7666.
48. Z. Gan, A. Zhao, M. Zhang, W. Tao, H. Guo, Q. Gao, R. Mao, and E. Liu, *Dalton Trans.*, 2013, **42**, 8597.
49. Z.-J. Jiang, C.-Y. Liu, and L.-W. Sun, *J. Phys. Chem. B*, 2005, **109**, 1730.
50. G. Niaura, A. K. Gaigalas, and V. L. Vilker, *J. Phys. Chem. B*, 1997, **101**, 9250.

Figure captions

Fig. 1 Schematic illustration for the preparation of Fe_3O_4@PANI@Au.

Fig. 2 TEM images of (a) Fe_3O_4 nanospheres, (b) Fe_3O_4@PANI, (c) Fe_3O_4@PANI@Au, (d-f) HRTEM images of Fe_3O_4@PANI@Au with different magnifications.

Fig. 3 XRD patterns of (a) Fe_3O_4 nanospheres, (b) Fe_3O_4@PANI (c) Fe_3O_4@PANI@Au.

Fig. 4 (A) EDX spectra of sample Fe_3O_4@PANI@Au. XPS spectra of Fe_3O_4@PANI@Au: (B) survey spectrum and (C) high-resolution XPS Au 4f spectrum in Fe_3O_4@PANI@Au.

Fig. 5 (A) FT-IR spectra and (B) Field-dependent magnetization of (a) Fe_3O_4 nanospheres, (b) Fe_3O_4@PANI (c) Fe_3O_4@PANI@Au.

Fig. 6 At 25 ^{o}C, UV-visible spectra of Congo red catalytically reduced by Fe_3O_4@PANI@Au composite in different concentration of $NaBH_4$ (10^{-3} mol/L). (A) 5.0, (B) 7.0, (C) 9.0. (D) First-order kinetic plot of Congo red reduction catalyzed by Fe_3O_4@PANI@Au composite. Data from Fig. 6C. Reaction condition:10 mg catalysts; 20 mL, 6.0×10^{-5} mol/L Congo red solution.

Fig. 7 (A) UV-vis spectra of high concentration of Congo red with the reduction of $NaBH_4$ in the presence of Fe_3O_4@PANI@Au catalyst at 25 ^{o}C, the solutions are diluted 10 times before test. (B) First-order kinetic plot of Congo red reduction catalyzed by Fe_3O_4@PANI@Au composite. Data from Fig. 7A. Reaction condition:10 mg catalysts; 20 mL, 6.0×10^{-4} mol/L Congo red solution; 9.0×10^{-3} mol/L $NaBH_4$.

Fig. 8 (A) Plot of the absorbance at λ_{max} of Congo red versus reaction time in different electrolytes; (B) Plot of the absorbance at λ_{max} of Congo red versus reaction time in different concentration of $NaNO_3$. Reaction condition: 25 ^oC, 10 mg Fe_3O_4@PANI@Au catalysts, 20 mL, 6.0×10^{-5} mol/L Congo red solution, 1.5 mL, 0.1 mol/L $NaBH_4$.

Fig. 9 Reduction kinetics of Congo red catalyzed by Fe_3O_4@PANI@Au composite in the presence of different surfactants (1×10^{-3} mol/L). Reaction condition: 25 ^oC, 10 mg Fe_3O_4@PANI@Au catalysts, 20 mL, 6.0×10^{-5} mol/L Congo red solution, 1.5 mL, 0.1 mol/L $NaBH_4$.

Fig 10 (A) Photo images of magnetically separating Fe_3O_4@PANI@Au composite from the reaction media after the reaction completion. Inset of Fig. 10A: TEM of Fe_3O_4@PANI@Au composite after five cycles of the catalysis reaction. (B) Changes in conversion of the substrates as the cycling continue. Reaction condition: 25 ^oC, 10 mg Fe_3O_4@PANI@Au catalysts, 20 mL, 6.0×10^{-5} mol/L Congo red solution, 1.5 mL, 0.1 mol/L $NaBH_4$.

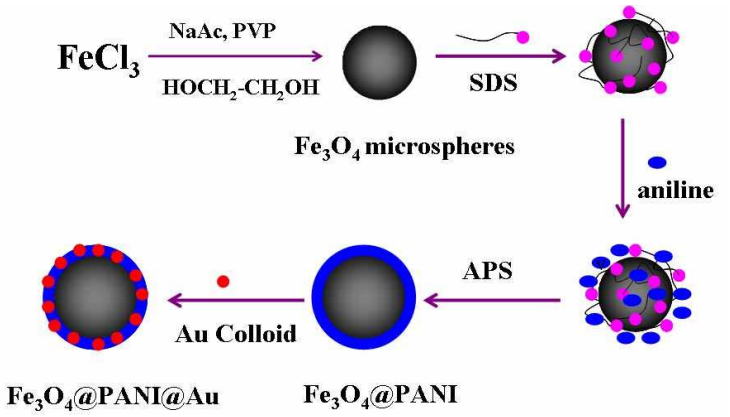

Fig. 1 Schematic illustration for the preparation of Fe_3O_4@PANI@Au.

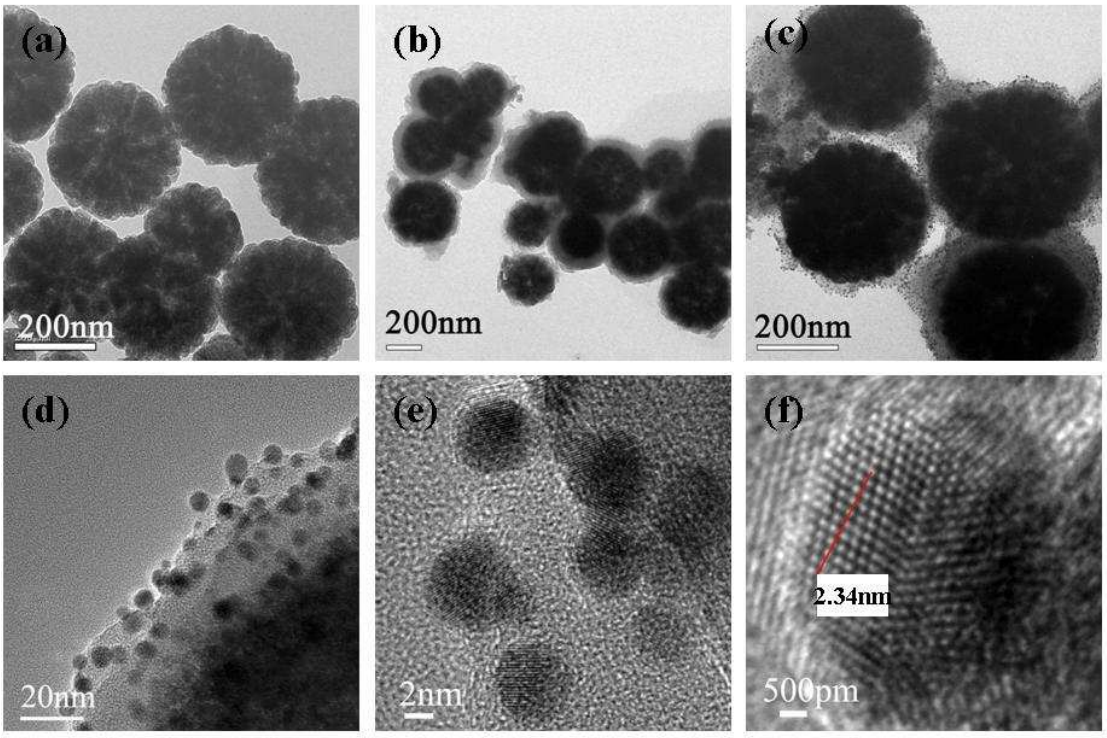

Fig. 2 TEM images of (a) Fe_3O_4 nanospheres, (b) Fe_3O_4@PANI, (c) Fe_3O_4@PANI@Au, (d-f) HRTEM images of Fe_3O_4@PANI@Au with different magnifications.

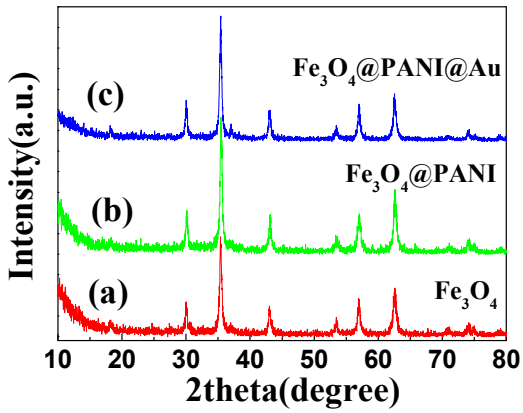

Fig. 3 XRD patterns of (a) Fe_3O_4 nanospheres, (b) Fe_3O_4@PANI (c) Fe_3O_4@PANI@Au.

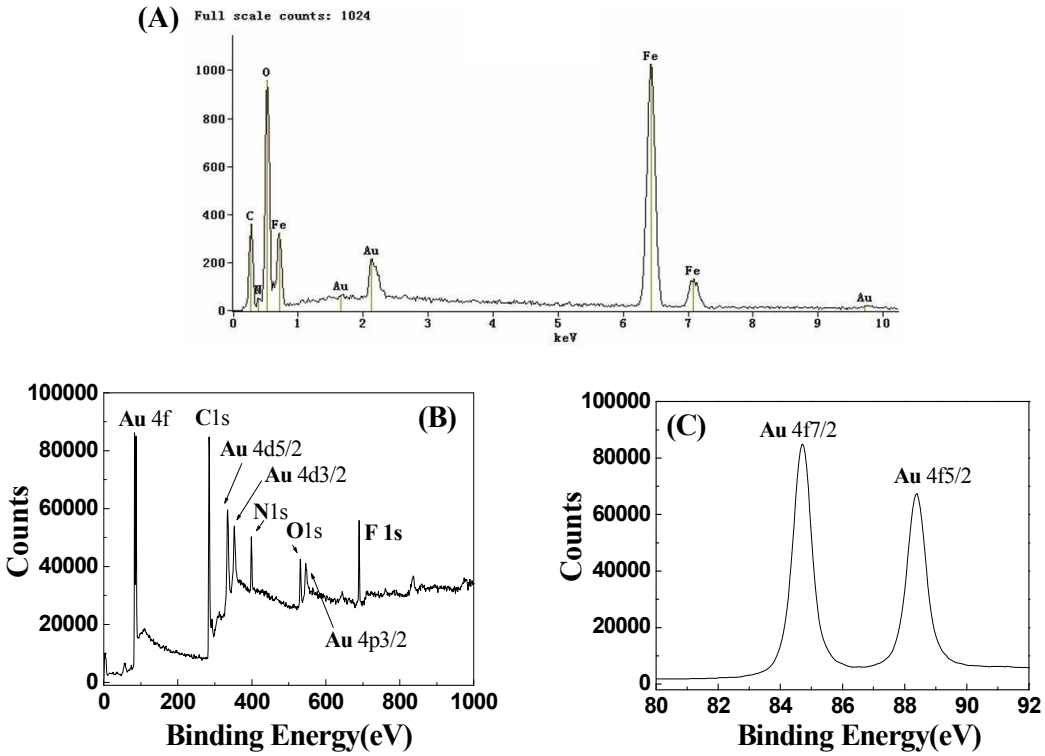

Fig. 4 (A) EDX spectra of sample Fe_3O_4@PANI@Au. XPS spectra of Fe_3O_4@PANI@Au: (B) survey spectrum and (C) high-resolution XPS Au 4f spectrum in Fe_3O_4@PANI@Au.

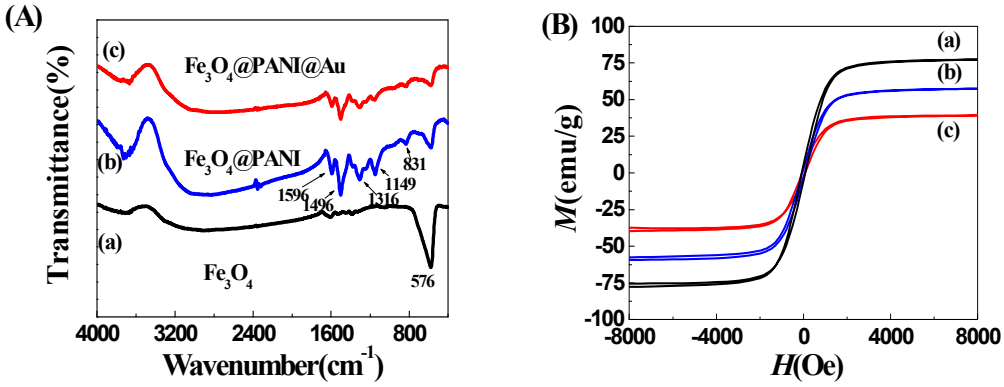

Fig. 5 (A) FT-IR spectra and (B) Field-dependent magnetization of (a) Fe_3O_4 nanospheres, (b) Fe_3O_4@PANI (c) Fe_3O_4@PANI@Au.

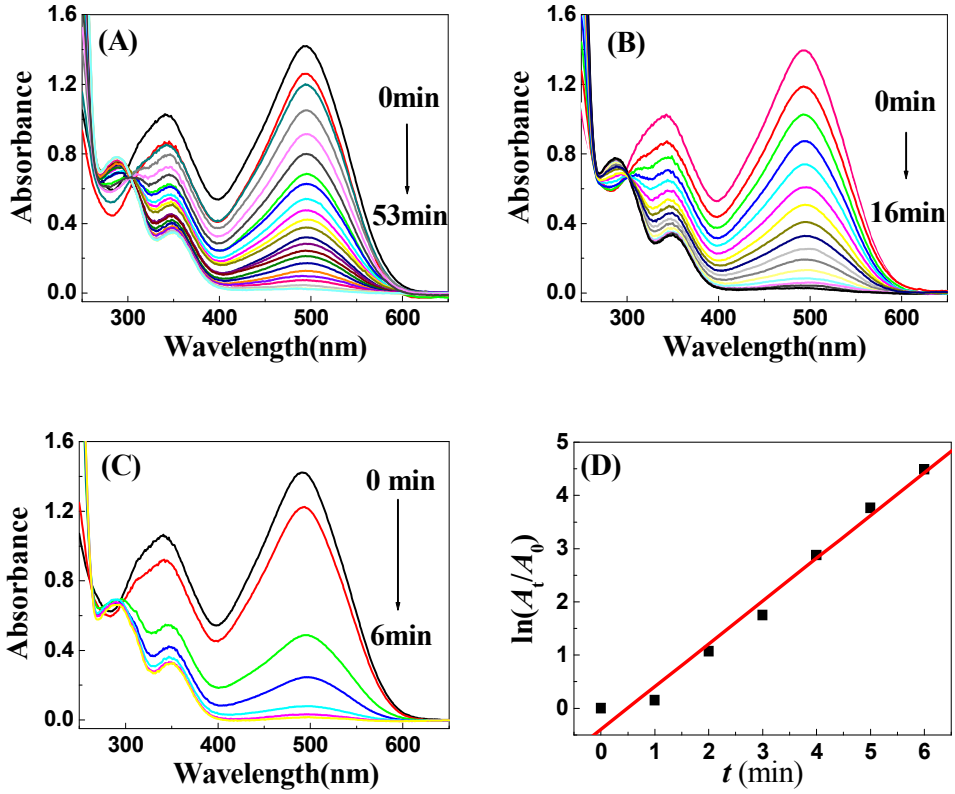

Fig. 6 At 25 °C, UV-visible spectra of Congo red catalytically reduced by Fe_3O_4@PANI@Au composite in different concentration of $NaBH_4$ (10^{-3} mol/L). (A) 5.0, (B) 7.0, (C) 9.0. (D) First-order kinetic plot of Congo red reduction catalyzed by Fe_3O_4@PANI@Au composite. Data from Fig. 6C. Reaction condition:10 mg catalysts; 20 mL, 6.0×10^{-5} mol/L Congo red solution.

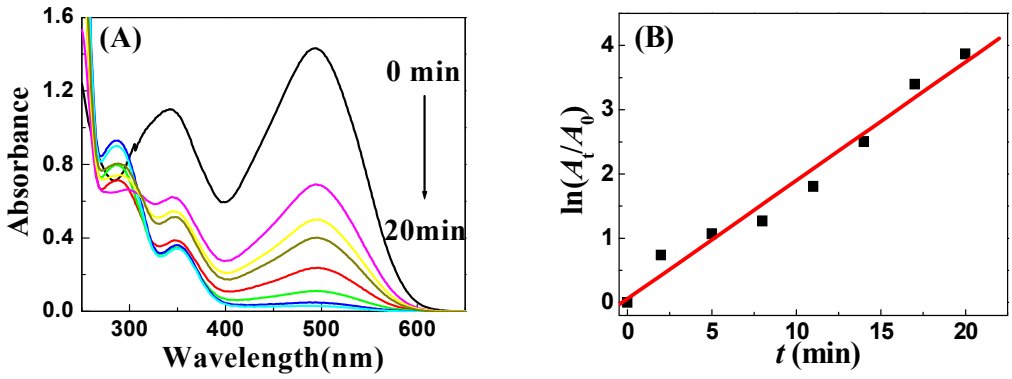

Fig. 7 (A) UV-vis spectra of high concentration of Congo red with the reduction of $NaBH_4$ in the presence of Fe_3O_4@PANI@Au catalyst at 25 ^oC, the solutions are diluted 10 times before test. (B) First-order kinetic plot of Congo red reduction catalyzed by Fe_3O_4@PANI@Au composite. Data from Fig. 7A. Reaction condition:10 mg catalysts; 20 mL, 6.0×10^{-4} mol/L Congo red solution; 9.0×10^{-3} mol/L $NaBH_4$.

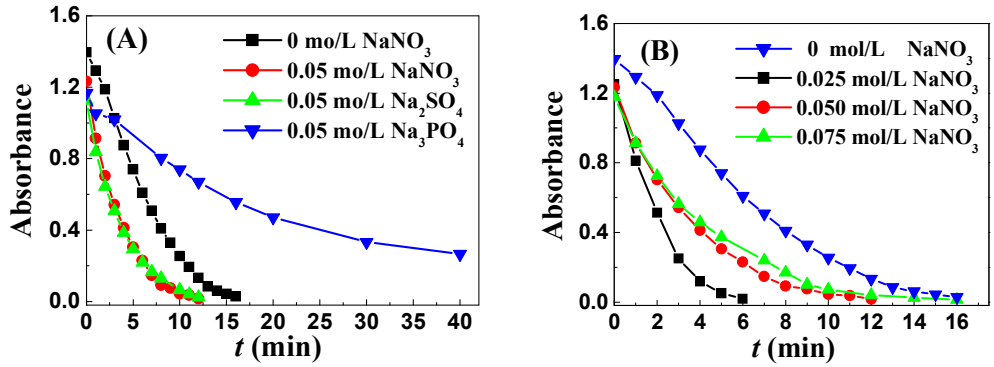

Fig. 8 (A) Plot of the absorbance at λ_{max} of Congo red versus reaction time in different electrolytes; (B) Plot of the absorbance at λ_{max} of Congo red versus reaction time in different concentration of $NaNO_3$. Reaction condition: 25 ^oC, 10 mg Fe_3O_4@PANI@Au catalysts, 20 mL, 6.0×10^{-5} mol/L Congo red solution, 1.5 mL, 0.1 mol/L $NaBH_4$.

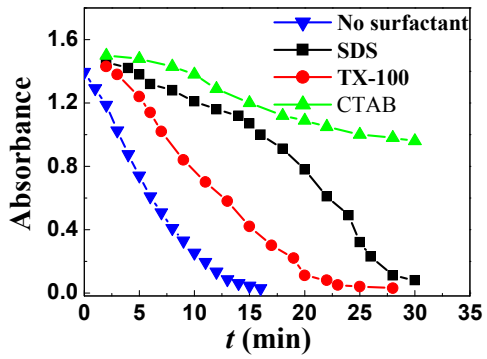

Fig. 9 Reduction kinetics of Congo red catalyzed by Fe_3O_4@PANI@Au composite in the presence of different surfactants (1×10^{-3} mol/L). Reaction condition: 25 ^{o}C, 10 mg Fe_3O_4@PANI@Au catalysts, 20 mL, 6.0×10^{-5} mol/L Congo red solution, 1.5 mL, 0.1 mol/L $NaBH_4$.

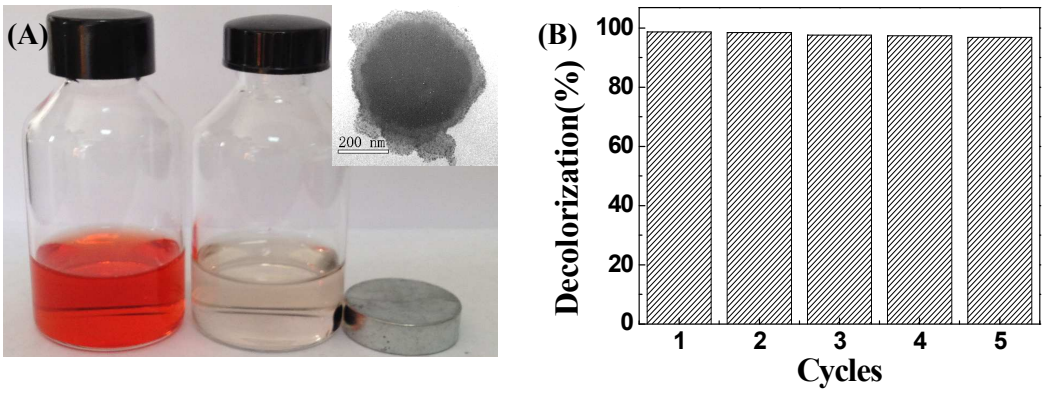

Fig 10 (A) Photo images of magnetically separating Fe_3O_4@PANI@Au composite from the reaction media after the reaction completion. Inset of Fig. 10A: TEM of Fe_3O_4@PANI@Au composite after five cycles of the catalysis reaction. (B) Changes in conversion of the substrates as the cycling continue. Reaction condition: 25 ^{o}C, 10 mg Fe_3O_4@PANI@Au catalysts, 20 mL, 6.0×10^{-5} mol/L Congo red solution, 1.5 mL, 0.1 mol/L $NaBH_4$.